Frustrated Magnetism in Vanadium Oxides

Burkhard Schmidt, Tetsuya Takimoto, Peter Thalmeier, and Victor Yushankhai

In magnetically frustrated compounds the pairwise exchange interactions of spins cannot all be minimized simultaneously in any microscopic moment configuration. This dilemma may already arise in the case of nearest neighbor interactions when the property of geometric frustration inheres in the lattice like in, e.g. trigonal, Kagomé, checkerboard or pyrochlore type lattices [1, 2]. In these cases the fundamental building blocks like triangles, plaquettes or tetrahedrons share common sites such that there is no unique state that minimizes all bond energies to nearest neighbor sites. Consequently, there will be many states which have approximately equally low energies, i.e., frustration leads to a large degeneracy of low lying states. This entails large quantum fluctuations which may prevent the appearance of magnetic order.

Frustration can also arise through the competition of longer range interactions even in simple structures like the two-dimensional (2D) square lattice. At low temperatures there are basically two alternatives: quantum fluctuations may select one of the degenerate states as the true magnetic state ('order by disorder') or they may lead to an ordered quantum phase with a new type of order parameter that is of the 'hidden order' type, i. e., it does not display a macroscopic modulation of the spin density.

In this report we first discuss the effects of frustration in the local moment J_1-J_2 model on the 2D square lattice. Here, we use both exact diagonalization for finite clusters, the finite temperature Lanczos method (FTLM), as well as analytical spin wave methods. In particular, the high field magnetization and magnetocaloric effect in the various phases are investigated which are relevant for a class of layered vanadium oxide compounds. In addition, a theory for the itinerant frustrated 3d- heavy fermion compound LiV_2O_4 will be discussed. It is based on ab-initio LDA calculations and the self-consistent renormalization (SCR) approach. It will be used to explain inelastic neutron scattering results which give direct insight into the origin of frustration in this compound.

Fig. 1: Phases of the spin-1/2 2D square lattice J_1-J_2 model as function of ϕ or J_2/J_1. The FM, NAF and CAF order (arrows) have wave vectors $\mathbf{Q} = (0,0)$, $(1,1)$ and $(1,0)$ or $(0,1)$ (in units of π/a) respectively. The grey sectors (J_2/J_1 values indicated on the outside) represent the stacked-dimer phase (right sector) and the spin-nematic phase (left sector). The dotted line corresponds to experimental values $\Theta_{CW} = (J_1 + J_2)/k_B$ for the Zn compound [10] with two possible phases at ϕ_+ (CAF) and ϕ_- (NAF). Full circles refer to CAF phases determined by neutron scattering [11] (From Ref. [4]).

Frustrated J_1-J_2 magnetism on the square lattice

The idea of a possible RVB state in the cuprates has led to a search for quantum spin liquids in 2D antiferromagnetic $S = 1/2$ compounds. In reality, most of them exhibit an ordered state with either magnetic or exotic hidden order. In particular, the nearest-neighbor Heisenberg model on a square lattice has an antiferromagnetic ground state, the Néel state. A more general case is the 2D J_1-J_2 model [3, 4, 5, 6] with an additional next-nearest-neighbor exchange interaction J_2. Such a model has a control parameter J_2/J_1 which may destabilize the Néel state of the $J_2 = 0$ Heisenberg model. This leads to various other magnetically ordered or hidden order states comprising a rich phase diagram in the J_1-J_2 plane (Fig. 1). Such states also have an interesting behaviour in an external field depending on the amount of frustration controlled by J_2/J_1.

Recently, various layered vanadium compounds have been found which can be well described by

the J_1-J_2 model. They are of the type Li_2VOXO_4 (X = Si, Ge) [8] and $AA'VO(PO_4)_2$ (A, A' = Pb, Zn, Sr, Ba) [9, 10] and consist of V-oxide pyramid layers containing V^{4+} ions with $S = 1/2$. From the analysis of the zero-field thermodynamics like specific heat and susceptibility the frustration ratio J_2/J_1 may be obtained. However, an ambiguity remains [3] which can be resolved by diagnosing the high-field behaviour discussed below.

The 2D square lattice J_1-J_2 model in a magnetic field is given by

$$\mathcal{H} = J_1 \sum_{\langle ij \rangle_1} \mathbf{S}_i.\mathbf{S}_j + J_2 \sum_{\langle ij \rangle_2} \mathbf{S}_i.\mathbf{S}_j - h \sum_i S_i^z . \quad (1)$$

Here J_1 and J_2 are the two exchange constants per bond between nearest and next nearest neighbors on a square lattice, respectively, and $h = g\mu_B H$ where g is the gyromagnetic ratio, μ_B the Bohr magneton, and H the magnetic field density. The phase diagram is preferably characterized by introducing equivalent parameters $J_c = (J_1^2 + J_2^2)^{\frac{1}{2}}$ and the frustration angle $\phi = \tan^{-1}(J_2/J_1)$.

This model has three possible classical magnetic ground states (see Fig. 1) depending on ϕ: Ferromagnet (FM), Néel antiferromagnet (NAF) and collinear antiferromagnet (CAF) [3]. The influence of exchange frustration leading to enhanced quantum fluctuations is strongest at the classical phase boundaries where the CAF phase joins the NAF ($J_2/J_1 = 0.5$, $\phi \approx -0.15\pi$) or FM ($J_2/J_1 = -0.5$, $\phi \approx 0.85\pi$) phases. In fact, in these regions they destroy long-range magnetic order [3] and establish two new ordered states, namely a gapped columnar dimer state at the CAF/NAF boundary and a gapless spin nematic state at the CAF/FM boundary [5] as shown by the grey sectors in Fig. 1.

Specific heat and susceptibility, also in finite field, may be calculated for finite clusters using the FTLM method to evalutate their respective cumulant expressions [3]. Fig. 2 shows the field dependence of $C_V(T,H)$ as a function of the frustration angle ϕ at constant temperature $T = 0.2J_c/k_B$. The heat capacity is large in the disordered regions reflecting the high number of quasi-degenerate states. Around $J_2/J_1 = 1/2$ ($\phi/\pi \approx 0.15$), a two-ridge structure evolves with increasing field. Due to the smallness of the saturation field, we currently cannot decide whether such a structure also exists at the "mirrored" ($J_2 \to -J_2$) position in the phase diagram at $J_2/J_1 = -1/2$. When reaching the saturation field, the heat capacity drops and eventually vanishes due to the gap opening.
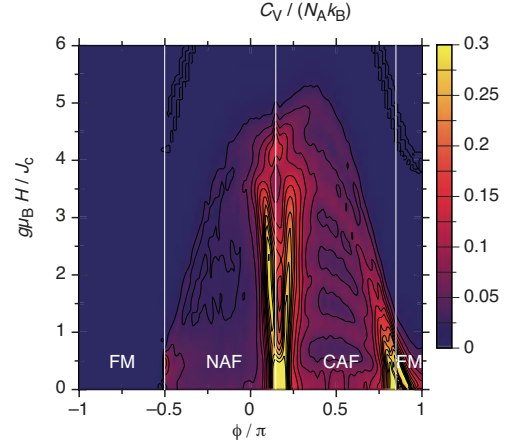
Fig. 2: *Contour plot of the heat capacity for the 24-site cluster at a fixed temperature $T = 0.2J_c/k_B$ as a function of the frustration angle ϕ and the magnetic field density H.*
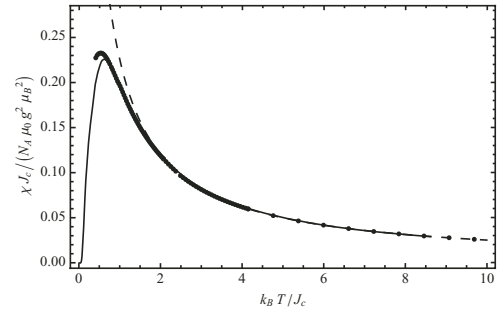
Fig. 3: *Temperature dependence of the magnetic susceptibility of $BaCdVO(PO_4)_2$. Dots denote the experimental result [7], the two curves denote a Curie-Weiss fit to the high-temperature part (dashed line) and a fit using our finite-temperature Lanczos data (solid line).*

The magnetic susceptibility and the magnetization at low temperatures of the new compound $BaCdVO(PO_4)_2$ have been measured [7]. Fig. 3 displays a plot of the temperature dependence of the magnetic susceptibility (dots) and a Curie-Weiss fit applied to the high-temperature part of the data (dashed line; $20\,K \leq T \leq 300\,K$). In addition, we have conducted a series of fits using our FTLM data calculated on a 24-site cluster [4]. The best fit is plotted in Fig. 3 (solid line). From this, we obtained a frustration angle $\phi = 0.77\pi$ and an effective exchange $J_c = 4.8\,K$. (The latter was used to normalize the experimental data for the plot.) This result is in excellent agreement with Ref. [7], where a high-temperature series expansion was used to determine the exchange constants.

Investigation of the uniform magnetization leads to a further understanding of the possible ground states of the model [6]. It may be obtained both
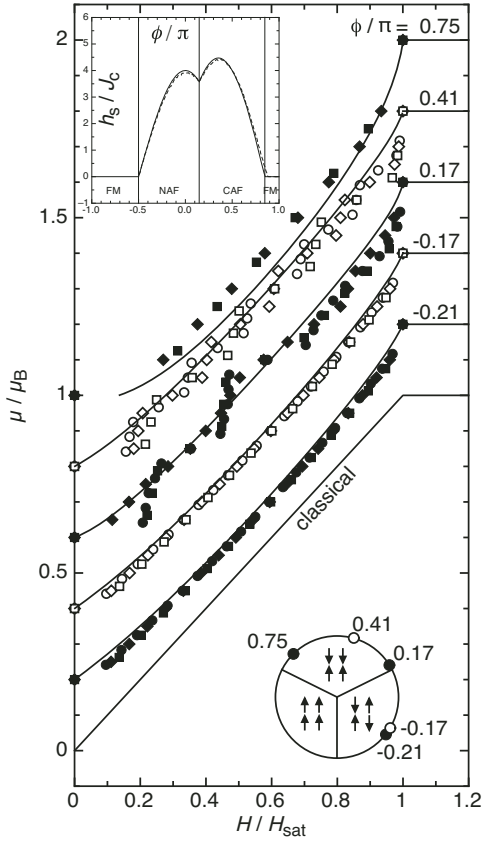
Fig. 4: Magnetization curves $\mu/\mu_B = gm \, (= m/S)$ for various ϕ in the AF or disordered sectors (each curve offset by 0.2). Symbols: $T = 0$ Lanczos results for $N = 16$ (squares), 20 (diamonds), 24 (dots, circles) size clusters. Lines: first order spin wave calculations. $\phi/\pi = 0.75, -0.21$ correspond to the possible CAF or NAF values of the Sr compound. Magnetization curves strongly differ in the extent of nonlinear deviation from the classical curve which corresponds to $\phi/\pi = -0.5$. Deep inside CAF or NAF regions the agreement of spin wave and Lanczos calculations is good. The values $\phi/\pi = 0.75, 0.17$ are nearby or within the non-magnetic sectors. At the CAF/NAF boundary the numerical data exhibit a plateau with $m/S = \mu/\mu_B = 0.5$ due to three-magnon bound states. Lower inset shows the position of plotted ϕ values in the phase diagram. Upper inset exhibits the saturation field as function of ϕ ($h_s \equiv g\mu_B H_{sat}$). (From Ref. [6]).

from numerical Lanczos calculations as well as analytical spin wave expansion starting from the three magnetic phases. In the latter approach the harmonic spin wave Hamiltonian is

$$\mathcal{H} = NE_0 + NE_{ZP} + \sum_{\mathbf{k}} \varepsilon_{\mathbf{k}}(h)\alpha_{\mathbf{k}}^{\dagger}\alpha_{\mathbf{k}} , \qquad (2)$$

where $\alpha_{\mathbf{k}}^{\dagger}$ creates magnons with a dispersion

$$\varepsilon_{\mathbf{k}}(h) = S(a_{\mathbf{k}} + c_{\mathbf{k}})^{\frac{1}{2}}(a_{\mathbf{k}} + c_{\mathbf{k}}\cos\theta_c)^{\frac{1}{2}} . \qquad (3)$$

With $\gamma_{\mathbf{k}} = \frac{1}{2}(\cos k_x + \cos k_y)$ and $\bar{\gamma}_{\mathbf{k}} = \cos k_x \cos k_y$,

the intra- and intersublattice interactions are given by $a_{\mathbf{k}} = 4[J_1 - J_2(1 - \bar{\gamma}_{\mathbf{k}})]$ and $c_{\mathbf{k}} = -b_{\mathbf{k}} = 4J_1\gamma_{\mathbf{k}}$, respectively, for the NAF and by similar expressions for the CAF [6]. The field-induced canting angle θ_c of sublattice moments (with respect to the field direction) decreases from $\theta_c = \frac{\pi}{2}$ to $\theta_c = 0$ when the field increases form zero to the saturation field $h_s(J_c, \phi)$ (see upper inset of Fig. 4).

The 'classical' canting angle obtained from minimization of $E_0(h, \theta_c)$ is given by $\cos\frac{\theta_c}{2} = h/h_s$ resulting in a linear magnetization $m_0 = S(h/h_s)$. This will be changed by the effect of zero point fluctuations which have an energy

$$E_{ZP} = \frac{1}{2N}\sum_{\mathbf{k}}[\varepsilon_{\mathbf{k}}(h) - Sa_{\mathbf{k}}] . \qquad (4)$$

The associated quantum corrections in the magnetization modify the linear classical behavior with a correction term $m_{ZP} = -\partial E_{ZP}(h)/\partial h$. It is determined by the dispersion $\varepsilon_{\mathbf{k}}(h)$ which becomes very anomalous at the classical phase boundaries CAF/NAF and CAF/FM [3]: The expression for the magnetization including quantum corrections up to order $1/S$ is given by [6]

$$m = S\frac{h}{h_s}\left[1 - \frac{1}{h_s}\frac{1}{N}\sum_{\mathbf{k}}c_{\mathbf{k}}\left(\frac{a_{\mathbf{k}} + c_{\mathbf{k}}}{a_{\mathbf{k}} + c_{\mathbf{k}}\cos\theta_c}\right)^{\frac{1}{2}}\right] . \qquad (5)$$

Because $h_s \sim S$ the second term in Eq. (5) is formally a $1/S$ correction to the linear classical term $m_0 = S(h/h_s)$. These corrections depend on the degree of frustration measured by ϕ. In the strongly frustrated regime around the classical phase boundaries the dispersion becomes flat along lines in the BZ [3]. Thus, there is a dramatic increase of the phase space for quantum fluctuations leading to strong nonlinear corrections for the magnetization (Fig. 4). Within the grey sectors of Fig. 1 magnetic order breaks down and quantum fluctuations stabilize spin-nematic (left) and stacked-dimer (right) hidden order parameters.

Fig. 5 presents a plot of the experimental magnetization data [7], marked as open circles, and a plot of data derived from exact diagonalization (full symbols). The latter are determined from the zero-temperature field dependence of the magnetization for tiles of $N = 16$ (squares), $N = 20$ (diamonds), and $N = 24$ sites (dots). Except for low magnetic fields, and taking into account the finite-temperature rounding of the experimental data around the saturation field, the agreement with experiment is, again, excellent. From our values for J_c and ϕ stated
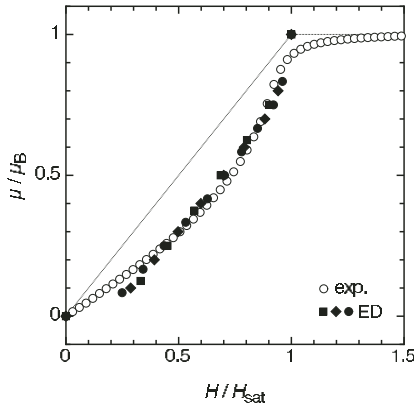
Fig. 5: Nonlinear magnetization curves due to quantum fluctuations both from experiment and theory (ED) with $\phi/\pi = 0.77$ for the BaCd-compound. It is closest to the spin-nematic sector in Fig. 1.
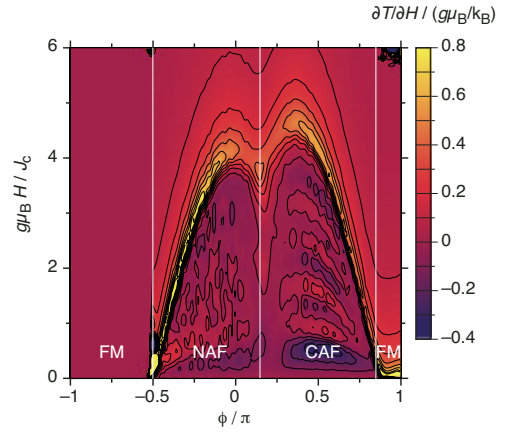

Fig. 6: Contour plot of the normalized magnetocaloric effect $\Gamma_{mc}/(T/H)$ for the 24-site cluster at a fixed temperature $T = 0.2 J_c/k_B$ as a function of the frustration angle ϕ and the magnetic field H.

above, we get a saturation field $H_{sat} = 4.1\,\text{T}$, compared to $H_{sat}^{exp} = 4.2\,\text{T}$ from Ref. [7]. The latter value gives a clear indication that $BaCdVO(PO_4)_2$, like $Pb_2VO(PO_4)_2$, is a collinear antiferromagnet since for the Néel phase, according to the inset of Fig. 4, the saturation field would be more than $50\,\%$ higher, namely $H_{sat}^{NAF} \approx 6.5\,\text{T}$.

Finite-size effects may play a role for the deviations of the two curves at low fields $H \leq 0.4 H_{sat}$: Experimentally, a linear, classical field dependence is observed at the lowest fields, whereas the finite-size gap and the corresponding Zeeman splitting of the ground-state doublet determines the nonlinear field dependence of the numerical values. We note that for a value $\phi = 0.77\pi$ (Fig. 5) close to the CAF instability a spin wave calculation for $M(H)$ no longer converges for small H [6]. Since the fully polarized state is an eigenstate of the Hamiltonian, finite size effects do not play a crucial role near the saturation field.

Further insight into the quantum phases of the J_1-J_2 model and its high-field behavior may be gained from magnetocaloric properties [4]. The magnetocaloric coefficient $\Gamma_{mc}(h)$ (the adiabatic cooling rate) has a sharp anomaly from which h_s may be obtained. It is defined as the rate of adiabatic temperature change with external field:

$$\Gamma_{mc} \equiv \left(\frac{\partial T}{\partial H}\right)_S = -\frac{T}{C_V}\left(\frac{\partial m}{\partial T}\right)_H . \qquad (6)$$

In a paramagnet one has $\Gamma_{mc}^0 = (T/H)$. Therefore, $\hat{\Gamma}_{mc} = \Gamma_{mc}/\Gamma_{mc}^0$ is the magnetocaloric enhancement due to spin interaction effects. For the

J_1-J_2 model, Γ_{mc}^0 may be again calculated numerically for finite clusters with the cumulant expression

$$\left(\frac{\partial T}{\partial H}\right)_S \bigg/ \left(\frac{T}{H}\right) =$$
$$-g\mu_B H \frac{\langle \mathscr{H} S_z^{tot}\rangle - \langle \mathscr{H}\rangle\langle S_z^{tot}\rangle}{\langle \mathscr{H}^2\rangle - \langle \mathscr{H}\rangle^2} . \qquad (7)$$

In Fig. 6, a contour plot of the normalized magnetocaloric effect as a function of the applied field h and the frustration angle ϕ is shown. The magnetocaloric enhancement ratio in FTLM and spin wave approximation (using Eqs. (5, 6)) exhibit qualitatively similar features: A strong upturn and a positive peak just above the saturation field h_s as well as for $T \ll J_c/k_B$ a negative coefficient immediately below h_s [4].

It is instructive to consider the dependence of $\hat{\Gamma}_{mc}(h = h_s; \phi)$ on the frustration angle keeping the field at saturation level where the maximum of Γ_{mc} occurs. Note that the specific heat $C_V(T, H)$ (Fig. 2) occurs in the denominator of Eq. (6). It shows a strong enhancement close-by and in the quantum phase regions ($\phi \simeq 0.15\pi, \phi \simeq 0.85\pi$) due to large degeneracy. This overcompensates the simultaneous increase of the numerator in Eq. (6). Therefore, the magnetocaloric enhancement $\hat{\Gamma}_{mc}$ is only moderate in these regions while its maxima occur in the middle of the NAF or CAF phase sectors of Fig. 1. The measurement of $\Gamma_{mc}(h)$ should be an excellent method to determine the saturation fields H_{sat} in the J_1-J_2 compounds. Their absolute values for the known layered V-oxides range from 5 to 25 T [4].
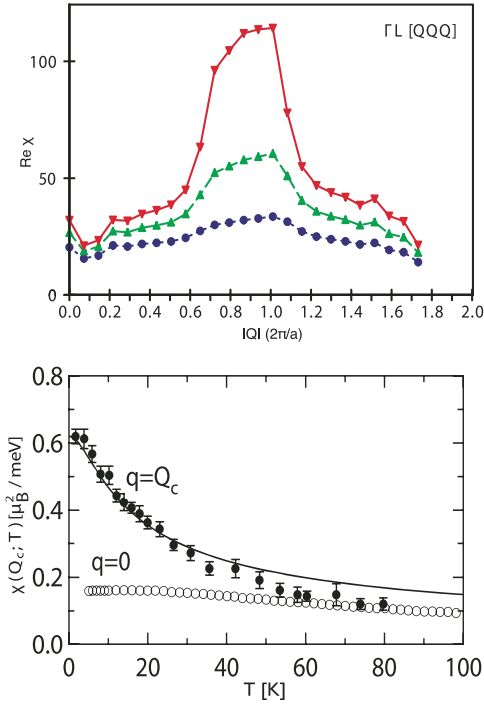
Fig. 7: Top (a): Static spin susceptibility $\chi(\mathbf{Q},0)$ *along* [111] *direction for different values of local exchange coupling constant* $K < K_c$ ($K = 0.45,\ 0.40,\ 0.30$ *from top to bottom). The critical exchange coupling is* $K_c = 0.49\,eV$ *and* $2\pi/a \simeq 0.76\AA^{-1}$. *(From Ref. [13]). Bottom (b): Static susceptibilities at* $q = Q_c$ *(full circles) and* $q = 0$ *(open circles) as functions of temperature observed in INS and magnetic measurements on* LiV_2O_4 *respectively. The solid line is a fit to* $\chi(Q_c, T)$ *using the self-consistent solution of* $y_{Q_c}(T)$. *(From Ref. [14]).*

Itinerant frustrated heavy fermion compound LiV_2O_4

The metallic spinel compound LiV_2O_4 is the first 3d- heavy electron system discovered [12]. Below 30 K, a large specific heat and Pauli susceptibility enhancement appears, the former yields $\gamma = C/T = 0.4\,\mathrm{J}/(\mathrm{mol\ K^2})$ at the lowest temperatures. Many proposals to explain this behavior have been put forward, including traditional Kondo-like scenarios. A special feature of the spinels and, therefore, of LiV_2O_4 is the fact that V atoms reside on a pyrochlore lattice. Their average electron count is $n_d = 1.5$ per V corresponding to quarter-filling (in the hole picture) of d-bands, i.e., the system is far from the localized Mott limit. Within RPA spin fluctuation theory based on ab-initio LDA electronic structure calculations it was found that pronounced short-range spin correlations in the paramagnetic metallic state of LiV_2O_4 appear.

The result of this calculation [13] for various sub-critical exchange strengths is depicted in Fig. 7 for the [111]-direction in **q**-space. Together with results for [100] and [110] it shows that the susceptibility is enhanced by approximately the same factor in a critical shell, which is a nearly spherical region with a radius $Q_c \simeq 0.6\,\AA^{-1}$ and a finite thickness $\delta Q \simeq 0.45\,\AA^{-1}$ in momentum space. This is the signature of frustration for itinerant spin-fluctuations. Since the static $\chi(\mathbf{Q}) \simeq \chi(Q_c)$ is almost degenerate in this shell, the system, although close to a magnetic instability, has no obvious way to select an ordering wave vector. As a consequence, the dynamical susceptibility resonds with slowing down (shifting the spectral function weight to very low energies) in the whole critical shell in the BZ. Therefore, there is a large phase space of low energy spin fluctuations which can renormalize the quasiparticle mass. This situation is quite different from non-frustrated lattices in which the enhancement of the interacting susceptibility is usually sharply peaked around the incipient magnetic ordering vector, providing only a small phase space and moderate quasiparticle mass enhancement.

When **Q** is located within the critical shell the dynamical susceptibility for low energy spin fluctuations is ($Q = |\mathbf{Q}|$)

$$\mathrm{Im}\,\chi(Q, \omega) \simeq z_Q \chi(Q)\omega/\Gamma(Q)\ , \qquad (8)$$

where $\Gamma(Q)$ and $z_Q < 1$ are their energy width and weight, respectively. Since $\chi(Q)$ is much enhanced and $\Gamma(Q)$ small in the critical shell the spectral function around Q_c is strongly peaked at low energies, in agreement with inelastic neutron scattering (INS) results [16, 17]. The conduction electrons are dressed with these low energy bosons leading to a large spin fluctuation specific heat $\gamma_{\mathrm{sf}} = C_{\mathrm{sf}}/T$ below 60 K given by

$$\gamma_{\mathrm{sf}} = \frac{k_B^2 \pi}{N} \sum_{\mathbf{q}} \frac{z(\mathbf{q})}{\hbar \Gamma(\mathbf{q})}\ . \qquad (9)$$

Since $\Gamma(\mathbf{q})$ is small in the whole critical shell around $|\mathbf{q}| = Q_c$ this may lead to a large γ_{sf}. The absolute scale of the spin fluctuation width Γ is estimated to fall between $0.5\,\mathrm{meV} < \Gamma < 1.5\,\mathrm{meV}$ with a corresponding γ_{sf} ranging between 100 and 300 in units of $\mathrm{mJ}/(\mathrm{K^2 mol})$. This proves that slow spin fluctuations over an extended momentum region, due to frustration, may explain the size of the large γ value in LiV_2O_4 and its heavy-fermion character.

At higher temperatures the spin fluctuation modes of different **q** are coupled leading to a transfer of

spectral weight from the critical region to the low-momentum region. Experimentally it was observed that above 60 K the susceptibility enhancement in the critical shell around $q = Q_c$ vanishes and becomes equal to the value at $q = 0$. The effect of mode coupling on the static susceptibility is described within Moriya's self-consistent renormalization (SCR) theory [18]. With $b(\omega) = 1/(e^{\omega/T} - 1)$ one finds

$$\frac{1}{\chi(\mathbf{q})_T} = \frac{1}{\chi(\mathbf{q})_0} + \frac{\bar{F}_{Q_c}}{N} \int_0^\infty \frac{d\omega}{2\pi} b(\omega) \sum_{\mathbf{q}'} \mathrm{Im}\, \chi(\mathbf{q}', \omega). \tag{10}$$

Here, $\bar{F}_{Q_c}$ is a mode-mode coupling constant for the critical shell. The reduced inverse susceptibility may be written as $y(Q_c, T) = 1/(2T_A \chi_{Q_c}(T))$ where $T_A \simeq 220$K is a scaling parameter. It is obtained from a numerical solution of the SCR integral equation derived from Eq. (10) [14, 15]. The resulting temperature dependence of the critical susceptibility $\chi_{Q_c}(T)$ together with corresponding experimental results and those of $q = 0$ are presented in Fig. 7b. It demonstrates that the critical enhancement of $\chi_{Q_c}(T)$ is rapidly reduced with temperature and approaches the value of the FM point $q = 0$. Since the ratio of scattering intensities at $q = Q_c$ and $q = 0$ is proportional to the square of the susceptibilities, Fig. 7b implies that the critical scattering intensity at Q_c is reduced by almost a factor 16 when the temperature increases to 60 K. Recently it was shown [15] that SCR theory can also explain the temperature and pressure dependence of the NMR relaxation rate in LiV_2O_4 sufficiently far from the quantum critical point where a yet unidentified order appears. Further investigations on the behavior of the resistivity of this compound are in progress.

References

[1] G. Misguich and C. Lhuillier in Frustrated Spin Systems ed. by H. T. Diep, World Scientific, Singapore, 2004.

[2] P. Fulde, P. Thalmeier, and G. Zwicknagl, Solid State Physics **60** (2006) 1.

[3] N. Shannon, B. Schmidt, K. Penc, and P. Thalmeier, Eur. Phys. J. B **38** (2004) 599.

[4] B. Schmidt, P. Thalmeier, and N. Shannon, Phys. Rev. B **76** (2007) 125113.

[5] N. Shannon, T. Momoi, and P. Sindzingre, Phys. Rev. Lett. **96** (2006) 027213.

[6] P. Thalmeier, M. Zhitomirsky, B. Schmidt, and N. Shannon, Phys. Rev. B **77** (2008) 104441.

[7] R. Nath, A. A. Tsirlin, H. Rosner, and C. Geibel, Phys. Rev. B **78** (2008) 064422.

[8] R. Melzi, S. Aldrovandi, F. Teboldi, P. Carretta, P. Millet, and F. Mila, Phys. Rev. B **64** (2001) 024409.

[9] E. E. Kaul, H. Rosner, N. Shannon, R. V. Shpanchenko, and C. Geibel, J. Magn. Magn. Mat. **272-276** (2004) 922.

[10] N. Kini, E. E. Kaul, and C. Geibel, J. Phys.: Cond. Mat. **18** (2006) 1303.

[11] M. Skoulatos, J. P. Goff, N. Shannon, E. Kaul, C. Geibel, a. P. Murani, M. Enderle, and A. R. Wildes, J. Magn. Magn. Mat. **310** (2007) 1257.

[12] S. Kondo et al, Phys. Rev. Lett. **78** (1997) 3729.

[13] V. Yushankhai, A. Yaresko, P. Fulde, and P. Thalmeier, Phys. Rev. B **76** (2007) 085111.

[14] V. Yushankhai, P. Thalmeier, and T. Takimoto, Phys. Rev. B **77** (2008) 094438.

[15] V. Yushankhai, T. Takimoto, and P. Thalmeier, J. Phys.: Cond. Mat. **20** (2008) 465221.

[16] A. Krimmel, A. Loidl, M. Klemm, S. Horn, and H. Schober, Phys. Rev. Lett. **82** (1999) 2919.

[17] S. H. Lee, Y. Qiu, C. Broholm, Y. Ueda, and J. J. Rush, Phys. Rev. Lett. **86** (2001) 5554.

[18] T. Moriya, Spin Fluctuations in Itinerant Electron Magnetism, Springer Ser. Solid-State Science **56** (1985).